NTNU – Trondheim
Norwegian University of
Science and Technology

Dynamic Modelling and Analysis of Submerged Floating Tunnels

Andreas Saur Brandtsegg

Civil and Environmental Engineering
Submission date: June 2012
Supervisor: Svein N Remseth, KT
Co-supervisor: Ragnar Sigbjörnsson, KT

Norwegian University of Science and Technology
Department of Structural Engineering

Department of Structural Engineering
Faculty of Engineering Science and Technology
NTNU- Norwegian University of Science and Technology

ACCESSIBILITY

Open

MASTER THESIS 2012

SUBJECT AREA:	DATE:	NO. OF PAGES:
Structural analysis	01.06.12	31 + 6 pages appendix

TITLE:

Dynamic Modelling and Analysis of Submerged Floating Tunnels

Dynamisk modellering og analyse av neddykkede rørbruer

BY:

Andreas Saur Brandtsegg

SUMMARY:

Investigations are performed on the capabilities of Computational Fluid Dynamics (CFD) to model a transient transcritical flow around a Submerged Floating Tunnel (SFT). The aim of this inquiry is to examine the possibility of modeling the effect of Vortex Induced Vibrations (VIV) on a circular cylinder, through a coupling between a 2D CFD simulation, and a 3D FEM analysis of the structure trough strip theory. To validate such an approach, it is essential to verify that the CFD analysis yields accurate results.

A simulation has been performed on the flow around a circular cylinder with $Re = 3.6 \cdot 10^6$, based on the solution of the 2D Unsteady Reynolds Averaged Navier-Stokes (URANS) equations with the Realizable k-ϵ turbulence model using enhanced wall treatment. The hydrodynamic values obtained is the time averaged drag coefficient ($C_{D,avrg}$), the root-mean-square lift coefficient ($C_{L,rms}$), and the non-dimensional shedding frequency (St). The analysis yields a $St = 0.26$, which is within published experimental values, in contrast to published numerically obtained results.

RESPONSIBLE TEACHER:	Svein Remseth
SUPERVISOR(S):	Svein Remseth, Ragnar Sigbjörnsson
CARRIED OUT AT:	Department of Structural Engineering

NTNU
Institutt for konstruksjonsteknikk

MSc thesis assignment 2012

Andreas Saur Brandtsegg

Dynamic modelling and analysis of submerged floating tunnels

Dynamisk modellering og analyse av neddykkede rørbruer

Dynamic simulations and analysis of the response of slender structures is an important theme within the field of structural dynamics. The interaction between the structure and environment is an important part of the dynamic modelling. The effects caused by the fluid are described by the general flow equations, and the appropriate turbulence model. The turbulence model is chosen based on the flow state caused by the problem at hand. This thesis will investigate the behaviour of the hydrodynamic loads on Submerged Floating Tunnels (SFT), with special emphasis of Fluid Structure Interaction (FSI) in marine environment.

The aim of this thesis is:

- To attain an understanding of the dynamic modelling of Submerged Floating Tunnels.
- To comprehend the theoretical background for Computational Fluid Dynamics (CFD), and demonstrate how CFD can be used to analyse the hydrodynamic effects caused by Fluid Structure Interaction (FSI).

The work should address the following topics:

- Introduction to Submerged Floating Tunnels
- Environmental loads and hydrodynamic effects caused by Fluid Structure Interaction
- Investigation of vortex induced vibrations (VIV) and their consequences for SFT
- Application of CFD to attain hydrodynamic coefficients describing the loads acting on a SFT with a circular cross section

The thesis must be executed according to the guidelines for master thesis laid down by the Department of Structural Engineering (see Department web site). Adaptions of the thesis should be considered accordingly to the nature of the problem.

Supervisor: Professor Svein Remseth

Research advisors: Ragnar Sigbjörnsson, Svein Remseth

The assignment should be submitted to the Department of Structural Engineering by June 11. 2012

NTNU, 1. March 2012

Preface

This paper is written as the final thesis of Andreas Saur Brandtsegg, for the master's degree program Civil and Environmental Engineering, on the spring 2012.

I took an interest in the field of CFD after working with dynamic structures subjected to sea loads in the pre works to this thesis [9]. I found that the approach used historically was to perform complex structural dynamic analysis and combine it with highly simplified hydrodynamic approximations. These models have several limitations and required unphysical assumptions with an unknown error estimate. When I started to performed inquiries around the clusters working on CFD I realized that there is segregation between the people working on fluid dynamics, and those working on structural dynamics. Few people were studying in the field of Fluid Structure Interaction (FSI), where the two are combined. This thesis is therefore written in the form of a paper such that hopefully more people can find the time to look at it, and investigate the possibilities that arises when combining the two fields of study.

I would like to thank Sigrid Kaarstad Dahl and Muk Chen Ong for their support in fashioning the Ansys Fluent simulation, Helge I. Andersson and Reidar Kristoffersen for valuable discussions on the subject of turbulence modeling, and my guidance counselors Ragnar Sigbjörnson and Svein Remseth for highly appreciated direction and support.

Trondheim

June 4, 2012

Andreas Saur Brandtsegg

Abstract

Investigations are performed on the capabilities of Computational Fluid Dynamics (CFD) to model a transient transcritical flow around a Submerged Floating Tunnel (SFT). The aim of this inquiry is to examine the possibility of modeling the effect of Vortex Induced Vibrations (VIV) on a circular cylinder, through a coupling between a 2D CFD simulation, and a 3D FEM analysis of the structure trough strip theory. To validate such an approach, it is essential to verify that the CFD analysis yields accurate results.

A simulation has been performed on the flow around a circular cylinder with $Re = 3.6 \cdot 10^6$, based on the solution of the 2D Unsteady Reynolds Averaged Navier-Stokes (URANS) equations with the Realizable k-ϵ turbulence model using enhanced wall treatment. The hydrodynamic values obtained is the time averaged drag coefficient ($C_{D,avrg}$), the root-mean-square lift coefficient ($C_{L,rms}$), and the non-dimensional shedding frequency (St). The analysis yields a $St = 0.26$ which is within published experimental values, in contrast to published numerically obtained results.

Sammendrag

Det er utført strømningssimuleringer for å undersøke om det er mulig ved hjelp av CFD (Computational Fluid Dynamics) å modellere transient strømning rundt en neddykket rørbru i det transkritiske området. Målet med dette er å finne ut om det er realistisk å modellere påkjenningene av virvelavløsninger, ved å benytte en kobling mellom 2D CFD simuleringer med en 3D struktur analyse ved bruk av stripeteori. For å kunne gjennomføre en slik analyse må det verifiseres at CFD simuleringen gir resultater med tilstrekkelig nøyaktighet.

Det ble derfor gjennomført en simulering av strømning rundt et sirculært tvernitt med $Re = 3.6 \cdot 10^6$*, hvor løsningen er basert på de todimensjonale URANS (Unsteady Raynolds Averaged Navier-Stokes) ligningene. Et transkritisk strømningsbilde krever at turbulens modelleringen blir foretatt av en forenklet turbulens modell på grunn av regnekapasitet. Analyser foretatt i denne oppgaven er gjennomført med en Realizale k-ϵ turbulens modell, med 'Enhansed' behandling av turbulens modeleringer nær overflaten av sylinderen. De hydrodynamiske resultatene som er hentet ut i fra analysene, er de statistiske gjennomsnitt verdiene av drag kreftene, og standard avviket av løfte kreftene, samt den dimensjonsløse virvelavløsnings frekvensen (St). Beregningene gir en* $St = 0.26$ *som er innenfor eksperimentelle verdier, i motsetning til hva som er oppnådd i allerede publiserte numeriske analyser.*

Contents

Figures

Tables

Nomenclature

Re	Reynolds number, ratio of inertial forces to viscous forces.
$C_{D,avrg}$	Time averaged drag coefficient
$C_{L,rms}$	Root mean square value of lift coefficient
St	Strouhal number, non-dimensional vortex shedding frequency
f_v	Vortex shedding frequency
D, d	Cylinder diameter
U_∞	Current inflow velocity
ρ	Fluid density
μ	Dynamic viscosity of the fluid
d_w	Wake width
C_p	Pressure coefficient
C_{pb}	Base pressure coefficient
T_v	Vortex shedding period
C_D	Drag coefficient
C_L	Lift coefficient
F_{x1}	Forces in current direction acting on the cylinder
F_{x2}	Forces normal to current direction acting on the cylinder
k	Turbulent kinetic energy
ϵ	Turbulent dissipation of kinetic energy
ω	Specific dissipation rate *(ϵ /k)*
y^+	Non-dimensional first node height
i, j	$i, j = 1,2$, where 1 is in current direction, and 2 is normal to current direction
u_i	Fluid velocity in specified direction
x_i	Spatial direction vector in specified direction

$\overline{u_i}$	Average fluid velocity
u_i'	Turbulent fluid velocity
ν	Kinematic fluid velocity (μ/ρ)
τ_t	Turbulent shear stress
ν_T	Turbulent kinematic viscosity
δ_{ij}	Kronecker delta function
Re_y	Reynolds number as a function of distance to nearest wall
I_u	Turbulence intensity
Δt	Non-dimensional time step
CFL	Courant number ($CFL = u\Delta t/\Delta x$)
Nc	Number of nodes in circumferential direction
Nt	Number of nodes in the direction normal to the cylinder wall
Φ_L	Fourier coefficient of the lift fluctuations
C_f	Skin friction coefficient
τ, τ_w	Skin friction on cylinder wall
θ_s	Separation angle
f_{body}	Body forces
$f_{surface}$	Forces acting on surface
p	Pressure
$\overline{p}$	Mean pressure
p'	Fluctuating pressure
ϕ	Velocity potential
ζ	Wave elevation as a function of time

Introduction

The Norwegian Public Road Administration is investigating the possibilities for extreme fjord crossings, with a width of the fjords in the range of 2 – 6 km, and a depth of more than 300m. A feasibility study is conducted in these days on crossing the Sognefjord, which are 3.7 km long and about 1250m deep, which is discussed in "A feasibility study – How to cross the wide and deep Sognefjord" [24]. One of the alternatives discussed for this kind of crossings is a Submerged Floating Tunnel (SFT). Such a bridge has yet to be built, and it would therefor involve several technological firsts. In 1998 a SFT was decided as the preferred solution for crossing the Høgsfjord, but was never built.

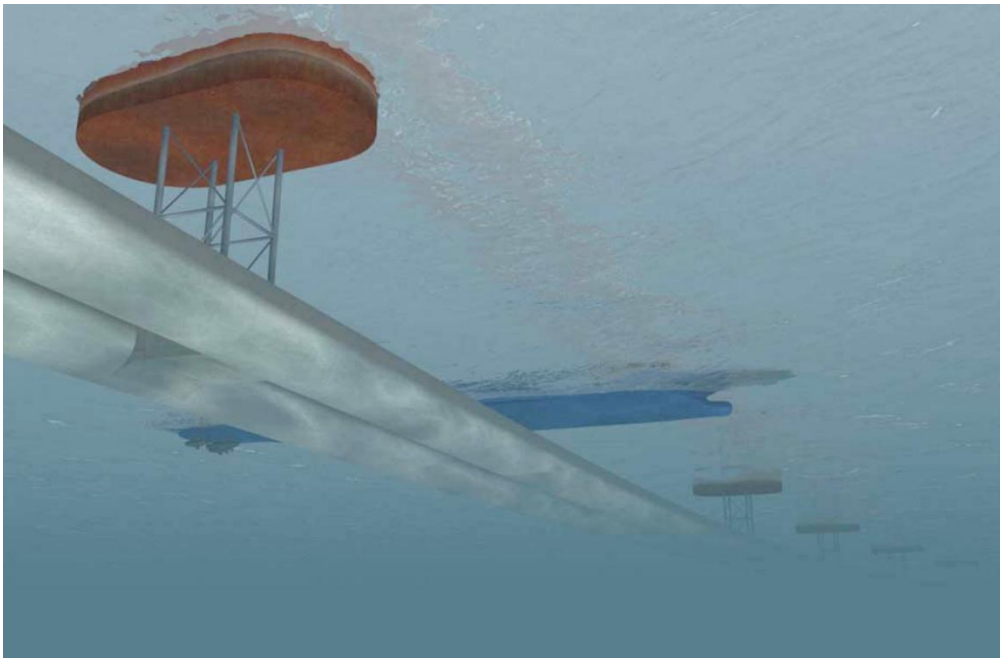

Figure 1: Illustration of a SFT concepts seen from underneath. [24]

A construction length of 3.7 km with no means for anchoring, due to the extreme depths, results in a very slender construction which is highly sensible to dynamic motions. The author has performed a dynamic modal response analysis of the Eigen modes and Eigen frequencies, in the pre works for this paper [9], which showed that several modes influence the response. More than thirty modes have significant modal mass, and a 3.7 km SFT would therefore have more than thirty Eigen frequencies, which suggests a significant possibility for resonance effects. A submerged floating tunnel would be submitted to multiple hydrodynamic effects. The present study will investigate the effect of current, caused by tides, acting on a submerged tunnel with circular shape.

Problem statement

Current past a circular cylinder results in a highly complex flow, involving instabilities such as wake separated shear layer and boundary layer. The boundary layer which is illustrated in Figure 2 is a thin layer between the separation points, which is close enough to the wall to be affected by viscous effects.

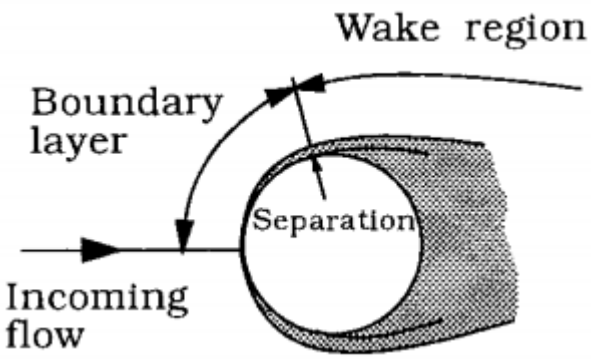

Figure 2: Definition sketch [33]

In the wake region vortexes cause pressure changes, which lead to fluctuations in the forces acting on the cylinder. Due to the unsymmetrical nature of the vortex shedding, forces normal to the current direction occurs. The forces normal to the current velocity vector are related to which side the vortex appears, while the inline forces are insensitive to the location of the vortex separation. This causes the inline forces to oscillate at half of the shedding period as discussed by Faltinsen [15]. Due to a larger period, the amplitude of the motions in the normal direction are usually twice the size of the inline amplitudes, and therefore often more critical. The frequency of which the vortexes occurs are denoted f_v, but are mostly referred to by the non-dimensional Strouhal number (*St*):

$$St = \frac{f_v D}{U_\infty} \qquad (1)$$

where D is the cylinder diameter, and U_∞ are the current velocity. All non-dimensional quantities describing a flow around a circular cylinder are dependent on the Reynolds number (*Re*) of the problem as stated in the book by Summer & Fredsøe [33], where:

$$Re = \frac{\rho D U_\infty}{\mu} \qquad (2)$$

ρ is the density of the fluid, and μ is the dynamic viscosity of the fluid.

The Strouhal number is influenced by the Reynolds number, as showed in Figure 3 by Schewe [27]. From the power spectres in Figure 3, one can also observe that not only does the value of St varies with Re, but also the nature of the vortex shedding. At $Re = 7.2 \cdot 10^5$ the shedding frequency has a wide power spectrum, while at both $Re = 1.3 \cdot 10^5$, and $Re = 7.1 \cdot 10^6$ the power spectres shows one distinct shedding frequency. This is important in dynamic analysis, because a narrow power spectra means that all the power is focused at one single frequency, and resonance effects can therefore be very damaging. The classification of shedding regimes indicated in Figure 3, and definitions of them are based by the work of Roshko [26], which investigated the transition in shedding regimes at Reynolds numbers from 10^6 to 10^7, and Schewes [27] paper on force fluctuations on circular cylinders.

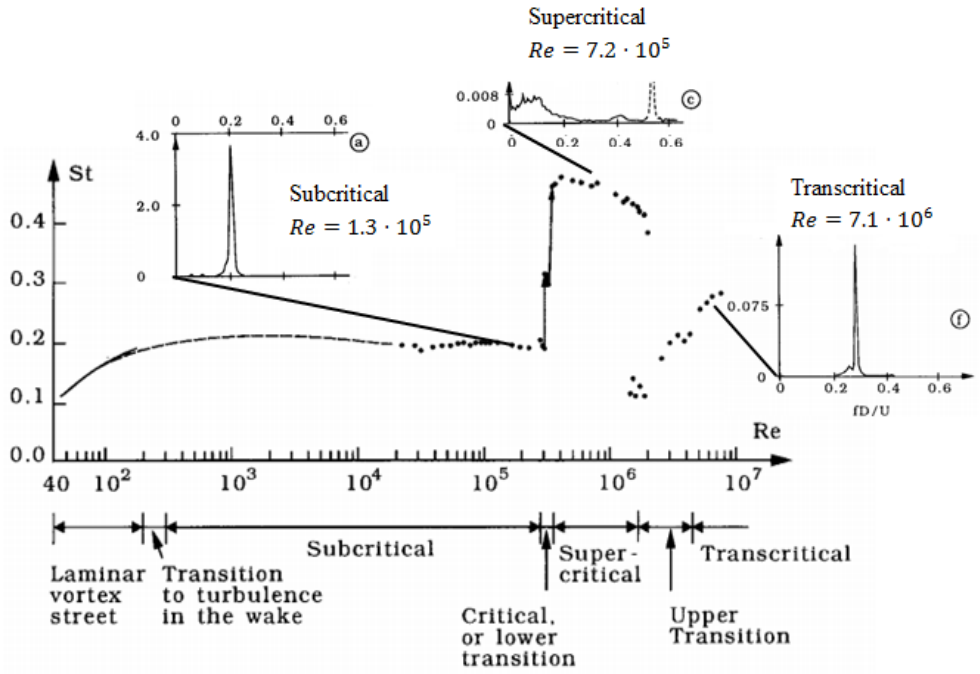

Figure 3: Strouhal number as a function of Reynolds number, and power spectra of lift fluctuations at indicated Re. [27]

The wake becomes turbulent already at $Re > 300$, but the boundary layer and the separation point remains laminar until $Re > 3 \cdot 10^5$. This region is called the subcritical shedding regime. At this flow regime the wake width (d_w) are larger than the cylinder diameter (d), as illustrated by Type A in Figure 4. The wake boundary in Figure 4 is identified by a constant pressure coefficient (C_p) equal to the base pressure coefficient (C_{pb}). The vortex shedding at this state occurs at one distinct frequency close to $St = 0.2$. When the Reynolds number is raised further above $3 \cdot 10^5$ the separation points oscillates between being laminar and turbulent. This occurs at $3 \cdot 10^5 < Re < 3.5 \cdot 10^5$, which is the critical regime. Above these values, the flow regime changes to supercritical.

Here, both separation points are turbulent, triggering a reattachment of the flow to the cylinder surface and the separation point to move backwards. This causes the wake width (d_w) to become smaller than the cylinder diameter (d), as illustrated by Type B in Figure 4. The area affected by the pressure drop behind the cylinder consequently becomes smaller; this causes a significant reduction in drag forces acting on the cylinder. This is referred to as the drag crises, which occurs in the supercritical regime ($3.5 \cdot 10^5 < Re < 1.5 \cdot 10^6$). When further increasing Re, the boundary layer becomes turbulent, first fluctuating between sides, until $Re > 3.5 \cdot 10^6$ where the boundary layer is turbulent on both sides. This is the transcritical regime. In this flow state the wake width increases compared to supercritical flow, but still remains smaller than the diameter of the cylinder (d_w<d).

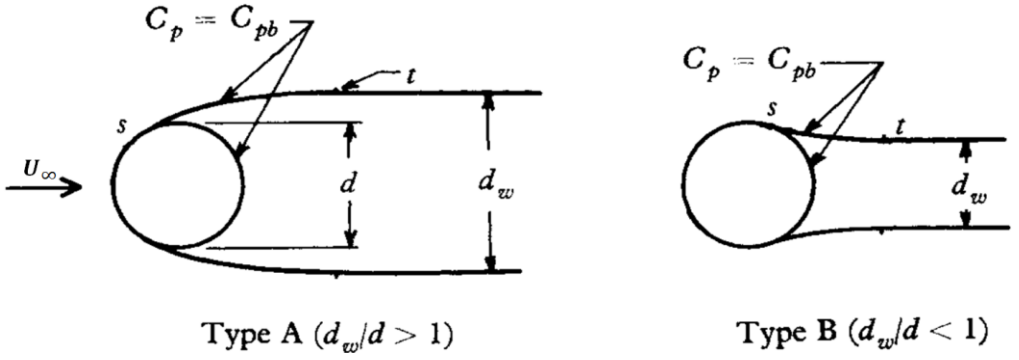

Figure 4: Free streamline model for relating base pressure coefficient to wake width. [26]

Flow around a circular cylinder is a classical case, which has been studied by several people, and a large amount of articles is written on the subject. However, the dimensions required for a submerged floating road tunnel can easily lead to Reynolds number in the area of $Re = 1.5 \cdot 10^7$, which is to the authors knowledge, higher than any published material. The reason for this lack in data can be illuminated by an example: If a wind tunnel tests should be performed with unpressurized air, and a structural diameter of 0.1m, the mac number of the air velocity must be approximately 7. This makes experiments extremely difficult to execute, and large measurement errors occurs. Because of this there is a wide spread in the experimental data published in the transcritical flow regime. The absence in reliable experimental data imposes a challenge for validating the obtained results. The reliability of the results presented in this paper are to be extensively discussed later on.

One of the most renown, and cited article on this subject is the article "On vortex shedding from smooth and rough cylinders in the range of Reynolds number $6 \cdot 10^3$ *to* $5 \cdot 10^6$" by Achenbach & Heinecke [2], which have

amongst other, studied the effect of the transitions between the subcritical, supercritical and the transcritical flow regimes. Their study obtained a $St = 0.25$ in transcritical flow. By the use of this, assumed tidal flow velocities between 0.25m/s and 2m/s, and cylinder diameter between 10-15m, the vortex shedding period can be approximated to:

$$T_v = \frac{St \cdot D}{U_\infty} \Rightarrow 10 seconds \; and \; 200 \; seconds \qquad (3)$$

This imposes a wide range of frequencies, which contains the natural frequencies one may presume a submerged floating tunnel to have.

Vortex shedding is a highly three dimensional effect, and have a small correlation length in the span direction of the cylinder. The correlation length for the transcritical regime is about 1-2D [16]. This would indicate low total forces on the structure caused by vortex shedding. However, motion of the structure can alter the nature of the vortex phenomena, and the frequency dependent added mass of the structure can be changed by the vortexes in such a way that the wet natural frequency of the structure and the shedding frequency moves towards each other, and a lock-in effect occurs. Lock-in between the vortex shedding and the motion of the structure; have been investigated by Sharpkaya & Shoaff [29]. They found that the correlation length increases significantly, the vortex strength increases, the motion amplitude rises which again causes a wider frequency band of which lock-in can occur. These properties make investigations of vortex induced vibrations vastly important when analysing dynamic behaviour in a slender structure, such as a submerged floating tunnel.

Due to the complexity of fluid structure interaction (FSI) and the immense computational resources it demands, few methods exist, which are based on sound physical principles, that can predict the occurring effects when a non-rigid cylinder is subjected to vortex induced vibrations. The methods used historically are based on complex structural finite element methods, and coupled with highly simplified empirical hydro dynamic models, such as Morris equation, or potential theory, (see appendix). More recently; attempts have been made to couple a structure analysis with a computational fluid dynamics (CFD) analysis by a strip method approach, like the work done by Schulz & Meling [28]. In their study of dynamic response of a marine riser, a 2D CFD analysis was coupled with a structural 3D FEM analysis with the use of strip theory, as illustrated in Figure 5. CFD analysis are based on solving the full Navier-Stokes equation (see appendix) to numerically simulate fluid flows.

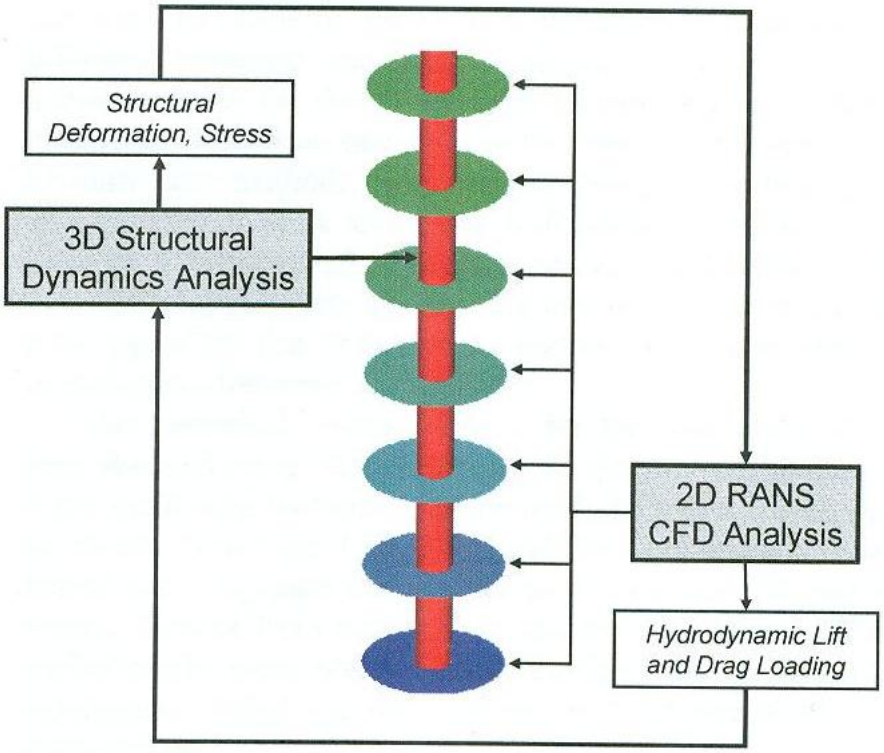

Figure 5: Outline of multi-strip flow structure coupling: multiple CFD slices provide the hydrodynamic loading along the span of the riser while a full 3D finite element method provides the riser displacement. [28]

These studies have given promising results capturing the effects taking place when a slender cylinder is exposed to current. These efforts have been made to model forces on marine raisers. The present problem however have much larger dimensions, as mentioned previously, and the flow is in the transcritical range. At high *Re* there is not possible to solve the Navier-Stokes equations directly, which is called the DNS method (Direct Navier-Stokes), due to extreme high computation costs. Therefore the turbulent contribution in the equation has to be estimated by a turbulence model. This yields also for a marine raiser, but the floating tunnel causes a different flow regime. The aim of this thesis is therefore to investigate the capability of CFD analysis to model the flow around a circular cylinder in the transcritical regime by the use of a suitable turbulence model.

To perform CFD analysis with Re higher than 10^6 is very costly in terms of computational time, it is therefore only in the present years that there have been published papers on this type of problem. Amongst the few papers published are the ones of Catalano et al. [12], Singh & Mittal [31], and Ong et al. [25]. Catalano et al. [12] compared the Large Eddy Simulation (LES), and an Unsteady Reynolds Averaged Navier-Stokes (URANS) simulation, and found that the LES gave inaccurate results for $Re > 10^6$, compared to existing experimental values. Singh & Mittal [31] investigated the relationship between

the drag crisis and the instability of the separated shear layer by the use of LES simulations. Both of these studies have investigated flow around a circular cylinder at $Re > 10^6$ but the only published data from this area is the drag coefficient at $Re > 4 \cdot 10^6$ from the URANS simulation of Catalano et al. [12]. The only numerically obtained comparison material on the Strouhal number in the transcritical regime, is the results of Ong et al. [25] performed at $Re = 3.6 \cdot 10^6$. The Strouhal number obtained here shows some discrepancy compared to experimentally obtained values. To be able to obtain the Strouhal number accurately is of high importance for a dynamic response analysis due to resonance effects.

The objective of the present study is therefore to investigate the ability of CFD analysis to model flow around a circular cylinder in the transcritical regime, and identify the issues such an analysis will impose. The tidal flow around a SFT may lead to $Re > 1.5 \cdot 10^7$, which is equivalent to a current velocity of $1.0[m/s]$. Simulations performed based such high Reynolds numbers will require more than one month of computation time for each simulation, on a powerful personal computer. The present simulation will therefore be performed with $Re = 3.6 \cdot 10^6$, which is still in the transcritical regime, and equivalent to a current velocity of $0.24[m/s]$. $Re = 3.6 \cdot 10^6$ is chosen due to comparison reasons. This is the same value used in the numerical analysis performed by Ong et al. [25] and the experiments executed by Achenbach [1], and Achenbach & Heinecke [2].

The CFD analysis provides a time series of force fluctuations acting on the cylinder, to best be able to compare results with other time series statistical coefficient on the forces is extracted. The hydrodynamic results extracted and compared with experimental data, and other numerical simulations, are the time-averaged drag coefficient, $C_{D,average}$, the root-mean-squared (standard deviation) lift coefficient, $C_{L,rms,}$ and the Strouhal number, *St*. The drag- and lift- coefficient, C_D and C_L respectively, are defined as:

$$C_D = \frac{F_{x1}}{0.5\rho U_\infty^2 D} \quad , \quad C_L = \frac{F_{x2}}{0.5\rho U_\infty^2 D} \qquad (4)$$

where F_{x1} represents the in the horizontal direction (along current direction), while F_{x2} represents the forces in the vertical direction acting on the cylinder. The values used to compere the present study against experimental values and previously performed numerically obtained results are the time average of C_D ($C_{D,average}$), and the root-mean-square value of C_L ($C_{L,rms}$).

Theoretical background

In the transcritical regime the periodic vortex shedding reappear and the von Karman vortex street is again distinct. It was therefore attempted to perform a LES, which was conducted based on the article of Breuer [10]. But it was found inaccurate for such high Reynolds numbers, as was also concluded by Catalano et al. [12]. A LES is a combination of DNS and RANS first proposed by Smagorinsky [32], where the large eddies, which are comparable in size to the characteristic length of the meant flow, are calculated by directly solving the Navier-Stokes equation, while the smaller eddies are modelled by a turbulence model. The most challenging concern in performing an analysis in the transcritical regime, is the comparison material, which is very slim at $10^6 <$ Re $<10^7$, and to the authors knowledge non-existent at $Re = 1.5 \cdot 10^7$. This is the reason why the most tested and documented turbulence simulation is applied, the $k-\epsilon$ model. The $k-\epsilon$ turbulence model is defined as a two equation model, where one equation describes the turbulent kinetic energy (k), and the other equation estimates the dissipation of turbulent kinetic energy (ϵ). The standard $k-\epsilon$ turbulence model was suggested by Launder & Spalding [20]. This is also the method used by Ong et al. [25] and Catalano et al. [12] which holds the numerical simulation performed with some of the highest Reynolds number published to days date. Due to a discrepancy between the obtained Strouhal numbers and experimental values in these analyses, the use of an improved k-ϵ method is suggested in this paper.

The standard k-ϵ turbulence model has proven to perform badly for near-wall problems of high Reynolds number flow as stated by Versteeg & Malalasekera [34]. These weaknesses appear for flow with high mean shear rates and at massive separations, which is present in the problem at hand. The turbulence model chosen is a modified k-ϵ suggested by Shih et al. [30]. This method improves the eddy viscosity equation used in the standard k-ϵ method in such a way that it no longer gives non-realizable stresses for large mean strain rates, which in some cases can be negative for the original method. The Realizable model contains a new equation for the turbulent dissipation of kinetic energy, which is based on the mean-square vorticity fluctuation. This is a non-linear turbulence model similar to the renormalization group (RNG) k-ϵ model applied by Tutar & Holdø [34]. Both the RNG and the realizable models outperforms the standard model when it comes to strong streamline curvature, vortices and rotation as found by Shih et al. [30]. This is effects which obviously plays an important role when analyzing vortex shedding around a circular cylinder. Tests was made to use curvature correction on the k-ϵ turbulence method to improve its known weaknesses to simulate flow around curves, but it was found that due to the fact that the realizable k-ϵ already contains terms to include rotational or swirl effects, curvature corrections is not

reliable for this problem, as stated in the Ansys theory guide [4]. Recent studies of Han et al. [17] have also shown that the Realizable k-ϵ turbulence model is much more insensitive to the inflow boundary conditions compared with the standard k-ϵ and the *k-ω* method. The *k-ω* turbulence method proposed by Wilcox [38], is a two equation model similar to the *k-ϵ* method, but instead of defining a turbulence dissipation a specific dissipation rate is defined ($\omega = \epsilon / k$). Since the practical problem most definitively not has deterministic inflow turbulence, the Realizable turbulence model is therefore a better choice when it comes to reliability for uncertain flow conditions. The Realizable $k - \epsilon$ is therefore applied in the present study.

The k-ϵ models are primarily valid for fully turbulent flows, and are therefore not applicable in the viscous affected near wall area, opposed to the k-ω which can be used throughout the boundary layer. Consequently the near wall must be dealt with in a separate manner. The standard wall function uses a formulation based on the logarithmic law for mean velocity, which is valid for $30 < y^+ < 60$, but is employed by CFD computer package Ansys Fluent for $y^+ > 11.225$, as stated in the theory guide by Ansys Inc [4]. The y+ value is a non-dimensional distance between the first node and the nearest wall, further defined in the appendix. This means that there is a discrepancy when $11.225 < y^+ < 30$, which is highly inconvenient for the present problem, which have a y^+ value that chances around the boundary of the cylinder, as shown in Figure 6. The large variations of y^+ around the cylinder surface can create quite large discrepancies, as illustrated by Benim et al. [7] in Figure 7, which shows the variations in drag coefficient when changing the *mean* y^+ value. Due to this limitation in the standard wall function, the enhanced wall function is applied in the present study. The enhanced wall function uses a combination of logarithmic law and linear laws of the wall, which is discussed later on in this paper. The optimal y^+ value for enhanced wall functions is *less* than 5, which is a one-sided domain, and can be for obtained for the entire surface of the cylinder.

Due to the fact that the k-ϵ is a purely 2D model, there is no reason for performing a 3D analysis, since this will not improve the results. The domain used is an elongated version of the domain suggested in Tutar & Holdø [34] and identical to the one used by Ong et al. [25].

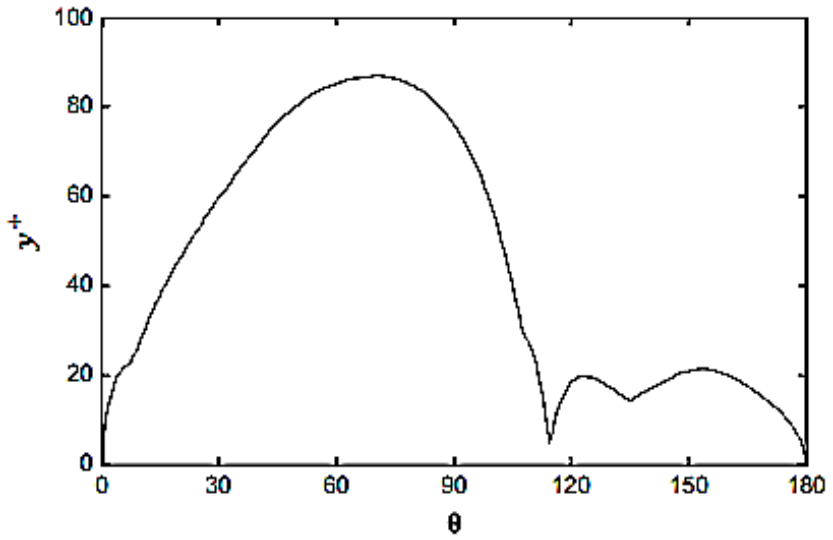

Figure 6: The variation of y+ around the cylinder. θ is the peripheral angle of the cylinder measured clockwise from the stagnation point. [25]

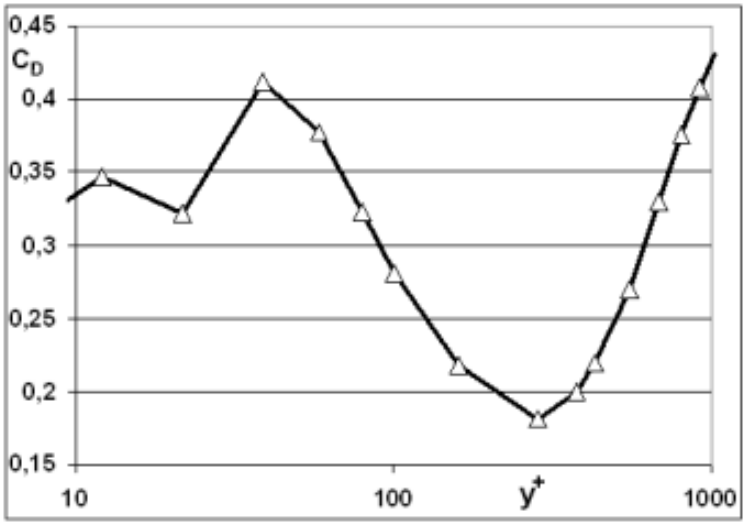

Figure 7: C_D as a function of average y^+ using standard wall-functions. [7]

Mathematical modeling

Realizeable k-ϵ

The equations needed to be solved by the CFD software for the present 2D problem is Reynolds equations for conservation of mass and momentum, which are derived in the appendix.

$$\frac{\partial \overline{u_i}}{\partial x_i} = 0 \qquad (5)$$

$$\frac{\partial \overline{u}_i}{\partial t} + \overline{u}_j \frac{\partial \overline{u}_i}{\partial x_j} = -\frac{1}{\rho}\frac{\partial \overline{p}}{\partial x_i} + \nu \frac{\partial^2 \overline{u}_i}{\partial^2 x_j} - \frac{\partial \overline{u_i' u_j'}}{\partial x_j} \qquad (6)$$

where i,j=1,2, and u_1 and u_2 are the velocities in horizontal and vertical direction respectively, $\overline{u}_i$ is the averaged velocity, $\overline{p}$ is the averaged dynamic pressure, ρ is the fluid density, and ν is the kinematic viscosity of the fluid. u_i' is the turbulent part of the velocities, and $\overline{u_i' u_j'}$ is the Reynolds stress tensor.

The only unknown in equation (6) is the Reynolds stress, which in turbulence modelling can be estimated by the Boussinesq approximation, which yields that there is a proportional relation between the turbulent stresses, and the gradient of the mean velocities:

$$\tau_t = -\rho \overline{u_i' u_j'} = \rho \nu_T \left(\frac{\partial \overline{u_i}}{\partial x_j} + \frac{\partial \overline{u_j}}{\partial x_i} \right) - \frac{2}{3}\rho k \delta_{ij} \qquad (7)$$

τ_t is the averaged turbulent stresses, δ_{ij} is the Kronecker delta function, and ν_T are the turbulent viscosity which are, unlike the kinematic viscosity, not a physical property, but varies inside the flow. When i = j, the turbulent stresses reduces to $-(2/3)\rho k$ where k is the mean kinetic energy in the turbulent motion, as described by Andersson et al. [3]. The Realizable $k-\epsilon$ turbulence model suggested by Shih et al. [30] estimates the mean kinetic energy from this equation:

$$\frac{\partial k}{\partial t} + \overline{u_j}\frac{\partial k}{\partial x_j} = \frac{\partial}{\partial x_j}\left(\frac{\nu_T}{\sigma_k}\frac{\partial k}{\partial x_j} \right) + \nu_T \left(\frac{\partial u_i}{\partial xj} + \frac{\partial u_j}{\partial x_i} \right) \frac{\partial \overline{u_i}}{\partial x_j} - \epsilon \qquad (8)$$

where ϵ is the dissipation of kinetic energy, and is found by solving the following equation:

$$\frac{\partial \epsilon}{\partial t} + \overline{u_j}\frac{\partial \epsilon}{\partial x_j} = \frac{\partial}{\partial x_j}\left(\frac{\nu_T}{\sigma_\epsilon}\frac{\partial \epsilon}{\partial x_j}\right) + C_1 S\epsilon - C_2\frac{\epsilon^2}{k+\sqrt{\nu\epsilon}} \qquad (9)$$

$$\sigma_k = 1, \qquad \sigma_\epsilon = 1.2, \qquad C_2 = 1.9,$$

$$C_1 = max\left\{0.43, \frac{\eta}{5+\eta}\right\}, \quad \eta = \frac{Sk}{\epsilon}, \quad S = \sqrt{2S_{ij}S_{ij}},$$

$$S_{ij} = \frac{1}{2}\left(\frac{\partial \overline{u_i}}{\partial x_j} + \frac{\partial \overline{u_j}}{\partial x_i}\right)$$

The turbulent viscosity (eddy viscosity) is given by:

$$\nu_T = C_\mu \frac{k^2}{\epsilon} \qquad (10)$$

The standard $k-\epsilon$ uses a constant C_μ, while the Realizable model uses the equation:

$$C_\mu = \frac{1}{A_0 + A_s\overline{u}^*\frac{k}{\epsilon}} \qquad (11)$$

$$\overline{u^*} = \sqrt{S_{ij}S_{ij} + \widetilde{\Omega}_{ij}\widetilde{\Omega}_{ij}}\ , \qquad \widetilde{\Omega}_{ij} = \Omega_{ij} - 2\epsilon_{ijk}\omega_k,$$
$$\Omega_{ij} = \overline{\Omega}_{ij} - \epsilon_{ijk}\omega_k, \qquad A_0 = 4.0,$$

where $\overline{\Omega}_{ij}$ is the mean rotation viewed in a rotating reference frame with the angular velocity ω_k.

$$A_s = \sqrt{6}\cos(\phi), \qquad \phi = \frac{1}{3}arc\cos(\sqrt{6}W),$$
$$W = \frac{S_{ij}S_{jk}S_{ki}}{\tilde{S}^3}, \qquad \tilde{S} = \sqrt{S_{ij}S_{ij}}$$

Near wall modeling

The enhanced wall function is applied as near wall treatment. This method is applicable to the laminar sublayer, buffer region, and fully turbulent region. The method is a combination of the linear, and the logarithmic laws of the wall. For $y^+ \approx 1$ the enhanced wall function will be identical to the traditional two layer wall function, which is formulated as follows:

In the viscous affected area, when Re_y as given in eq. (13) is smaller than 200, the one equation model of Wolfshtein [39] is applied. The kinematic turbulence equation is the same trough out the boundary layer. However the turbulent viscosity is modelled differently in the viscous affected boundary layer, where a two layer turbulence viscosity formulation proposed by Jongen [19] is implemented:

$$\nu_{T,2layer} = C_\mu l_\mu \sqrt{k} \qquad (12)$$

$$l_\mu = y c_l \left(1 - e^{-\frac{Re_y}{A_\mu}}\right), \qquad c_l = \kappa C_\mu^{-3/4},$$
$$\kappa = 0.41, \qquad A_\mu = 70$$

The enhanced wall function combines the two formulas of turbulent viscosity with a blending function which is dependent of:

$$Re_y \equiv \frac{y\sqrt{k}}{\nu} \qquad (13)$$

where y is the distance to the nearest wall. The criteria for the border of the viscous affected area are decided by the turbulent Reynolds number (Re_y). For $Re_y > Re_y^*$; where $Re_y^* = 200$, the realizable k-ϵ turbulence method, described earlier is applied. For $Re_y < Re_y^*$ the turbulence viscosity is a combination of the 2 layer, and the Realizable turbulence viscosity. These are combined by the following blending function:

$$\nu_{T,enhansed} = \lambda_\epsilon \nu_T + (1 - \lambda_\epsilon)\nu_{T,2layer} \qquad (14)$$

$$\lambda_\epsilon = \frac{1}{2}\left[1 + \tanh\left(\frac{Re_y - Re_y^*}{A}\right)\right], \qquad A = \frac{|\Delta Re_y|}{\tanh(0.98)} \qquad (15)$$

$$\Delta Re_y \; is \; between \; 5\% - 20\% \; of \; Re_y^*$$

The turbulent dissipation is given by this equation:

$$\epsilon = \frac{k^{\frac{3}{2}}}{l_\epsilon} \qquad (16)$$

$$l_\epsilon = yc_l\left(1 - e^{-\frac{Re_y}{A_\epsilon}}\right),\ A_\epsilon = 2c_l$$

The use of a wall function which is applicable for y+ values inside the wall buffer region, improves the accuracy for flow around the cylinder, which have a highly varying y+ value around the boundary.

Numerical solution technique

The domain used in these analyses is an elongated version of the domain used by Tutar & Holdø [34], which was proposed by Ong et al. [25] The domain size is 27D in the flow direction and 14D in the transverse direction. The boundary conditions are also identical to the ones used in Ong et al. [25] to achieve good conditions for comparing these results. The boundary conditions are shown in Figure 8, and are based on a turbulence intensity ($I_u = u_1'/U_\infty$) of 0.8%, and a non-dimensional length scale (L/D) of 0.0045. The turbulence intensity is chosen to best be able to compare results to the ones obtained by Ong et al. [25] which applied 0.8% in his simulation, and Achenbach [1] which obtained 0.7% in his wind tunnel test. As mentioned previously, the Realizeable k-ϵ turbulence method is quite insensitive to the inflow conditions, and should therefore not be very influenced by them as discussed by Han et al. [17]. The solver used in the simulation is the Pressure-Implicit with Splitting of Operators (PISO) scheme implemented in Fluent, which have shown to be accurate and robust for transient flows as discussed by Barton [6]. The numerical method is of first order in time and second order in spatial discretization. The time step used is a non-dimensional time step of $\Delta t=0.001D/U_\infty$, which imposes a CLF number ($CLF = u\Delta t/\Delta x$) of less than one for all simulations

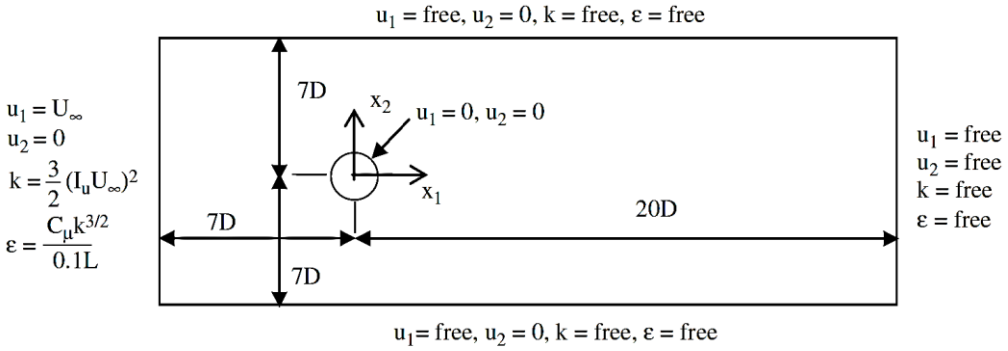

Figure 8: The size of the computational domain and the imposed boundary conditions. [25]

The enhanced wall treatment demands a low y+ value ($y^+ < 5$) as found by Coussirat [13], which leads to a significant mesh refinement compared to a standard wall function analysis. A mesh test was therefore conducted to find a suitable combination of accuracy and computation time. The coarsest mesh used in these analyses contains twice the number of elements compared to the mesh used by Ong et al. [25].

Table 1: *Data concerning the meshes used in convergence study.*

Mesh	Elements	Y+	Nc	Nt	Aspect ratio	$C_{D,avrg}$	$C_{L,rms}$	St
M1	110,000	10	600	150	73	0.3792	0.1281	0.3357
M2	110,000	5	600	150	140	0.3885	0.1446	0.2997
M3	110,000	2.5	600	150	293	0.3798	0.1443	0.3452
M4	206,000	2.5	1200	150	147	0.3706	0.1339	0.2572
M5	228,000	4	1080	200	100	0.3779	0.1352	0.2582

Nc is the number of nodes in the circumferential direction. Nt is the number of nodes normal to the cylinder wall. Aspect ratio is the highest relation between the height and width of an element, found in the mesh.

The meshes M1-3 have the same number of elements, but the y+ value is changed by varying the size relation between the first and last element in the direction normal to the cylinder wall. When inspecting the Strouhal numbers with the respect of y+ values shown in Figure 9 it is clearly illustrated that the y+ value is not the only parameter that influences the analysis.

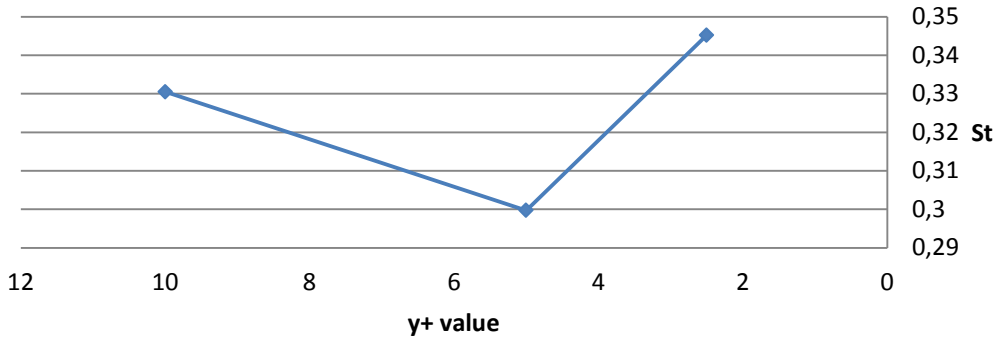

Figure 9: Convergence study for Strouhal numbers for meshes M1-3 with the respect of y+ value

The relation between height and width of one element is called the aspect ratio. When changing the y+ value in such a manner, the aspect ratio also changes, which could affect the result. The analysis of the M4 mesh is conducted to investigate the effect the aspect ratio has on the solution. The aspect ratio in M4 is almost the same as in M2; this is achieved by doubling the number of nodes in the circumferential direction of the cylinder. The analysis performed on the M4 mesh shows a significantly influence on the Strouhal number by the aspect ratio. To reduce the aspect ratio comes at the price of increasing the number of elements, which raises the computation costs. The computation time needed to perform the analysis on M4 is more than 100 hours on an Intel Core i5-2410M CPU. To execute a full mesh test on aspect ratio, y+ value and amount of elements is too time consuming to be executed during this master thesis. Instead, a mesh (M5) was fashioned to fit the criteria's given in the Fluent user guide by Ansys Inc. [5], and confirmed by literature, [13] [21]. High aspect ratios are not preferable, but are unavoidable in this analysis. Quadrilateral elements which are used in the present study can handle higher

aspect ratios compared to other element shapes. Also the use of double precision in the solver reduces high aspect ratio errors. The Ansys user guide suggests that the aspect ratio should not be larger than 100 in the boundary region, for such a problem. However Mittal [21] investigated the performance of high aspect elements on flow past a circular cylinder, and found that quadrilateral elements with an aspect ratio as high as 10^3 yielded acceptable results for the Strouhal number, and both drag and lift-coefficients. The reason why it can be so high in this area is that the rate of change is much lower in the circumferential direction compared to the normal direction in the boundary layer zone. In the domain however, the aspect ratio should not exceed five. The M5 therefor contains an aspect ratio lower than 100 in the boundary layer, and less than 5 in the rest of the domain. The first node height is 0.003% of the cylinder diameter, and was chosen as such that the y+ value is lower than five along the entire cylinder wall, as shown in Figure 10. The use of a maximum y^+ value below five have been validated by Coussirat [13]. Figure 11 shows the grid used in M5. Despite the quite brute and unscientific alterations between M4 and M5, the analysis yield small differences. The results in time averaged drag coefficient $C_{D,average}$ obtained from M4 and M5 differs 1.9%, while the Strouhal number (St), and the root-mean-square lift coefficient $C_{L,rms}$ differs 0.4% and 0.9% respectively. These results are satisfactory for the present investigation. The results from M5 is therefore chosen as the most reliable, and used for further comparisons.

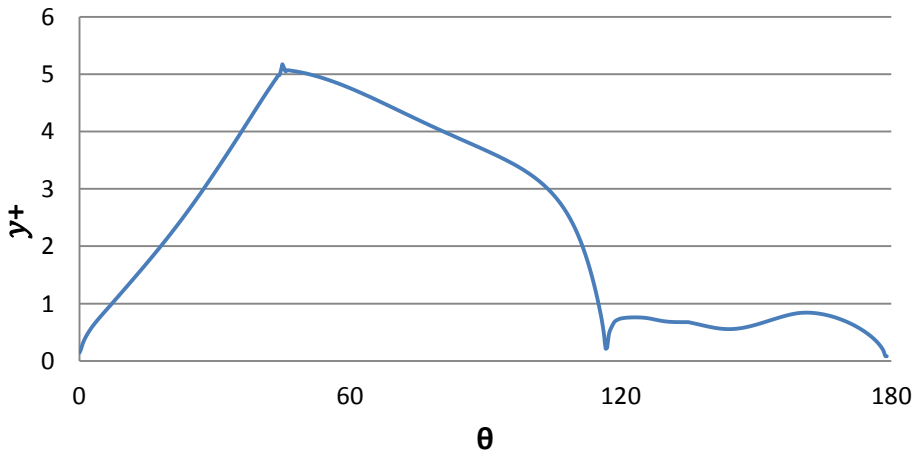

Figure 10: y+ value around the cylinder wall, with respect to the peripheral angle θ measured from the stagnation point.

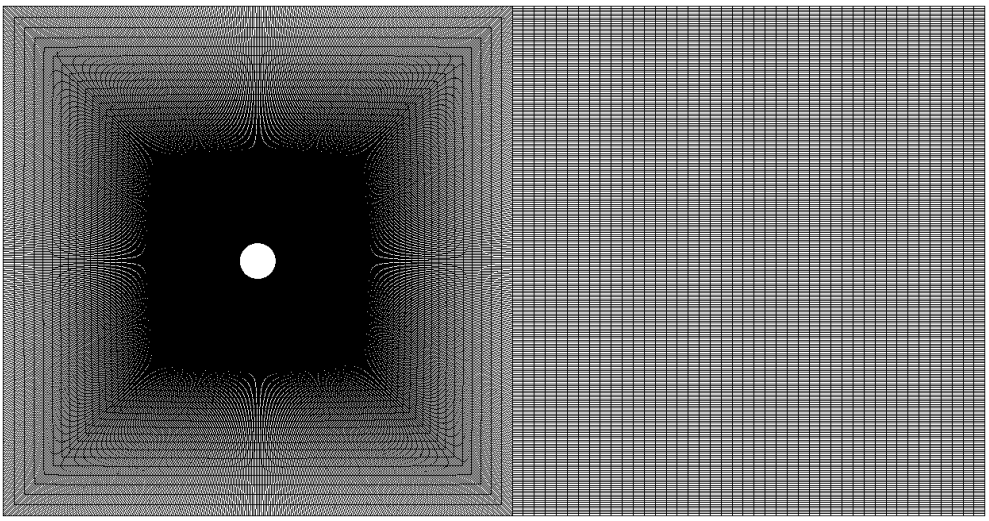

Figure 11: The M5 mesh chosen for the comparison.

Results and discussion

Transient simulations have been performed on the flow past a circular cylinder in the transcritical flow regime at $Re = 3.6 \cdot 10^6$. The turbulence model used is the Realizable k-ϵ method with enhanced wall treatment. The analysis have been simulated a 150 non-dimensional time steps, and the results have been obtained from the last 50 time units. The computation has been performed with a CFL number below 1. The hydrodynamic quantities that are extracted are the time averaged drag coefficient $C_{D,avrg}$, the root mean square lift coefficient $C_{L,rms}$, and the non-dimensional shedding frequency St. To investigate the reliability of the CFD analysis in the transcritical regime, $C_{D,avrg}$, $C_{L,rms}$, and St is compared to experimental data [1] [2] [18] [26] [27] [40] and numerical simulation [25] [12]. Key data is presented in *Table 2*. The values obtained in the present simulation are well within the published experimental values which have a large spread. There are no published numerical simulations to the author's knowledge that have been able to obtain a Strouhal number within the range of experimental values. It is therefore very interesting (and pleasing) to observe that the present simulations are able to achieve this. The hydrodynamic quantities presented in this paper are obtained from the time series of the force coefficients which is illustrated in Figure 12.

Table 2: *Existing data of comparison at* $Re = 3.6 \cdot 10^6$

	$C_{D,avrg}$	$C_{L,rms}$	St
Present simulation	**0.3779**	**0.1352**	**0.2582**
Ong et al.	0.4573	0.0766	0.3052
Catalano et al. $Re = 4 \cdot 10^6$ URANS	0.46	-	-
Benim et al. URANS	0.38		
Achenbach & Heinecke (1980)	0.70	-	0.25
Published experimental data	0.36 - 0.75	0.06 - 0.14	0.17 - 0.29

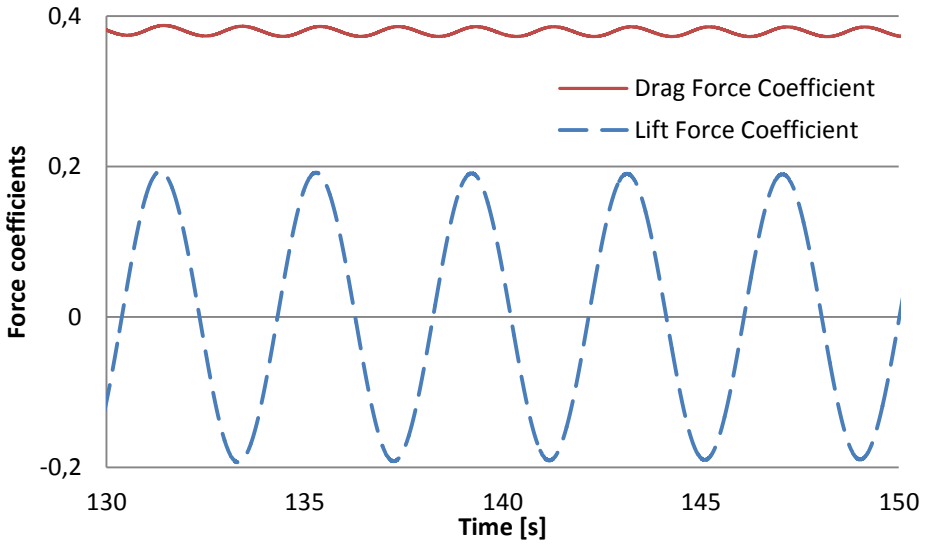

Figure 12: Time series of the force coefficients obtained from the CFD analysis.

Figure 13 show drag coefficients from experimental results extracted from Bohl & Elemendorf [8], and the numerical predictions of Benim et al. [7] from their k-ϵ simulation, and their SST simulation. SST is an improved k-ω turbulence model. The numerically obtained drag coefficient is coherently with the present simulation, but all numerical results under predicts the measurement. This is suggested by Benim et al. [7] to be caused by the difficulties in modelling the organized transient motions for the smaller eddies. The averaging performed in the turbulence model causes information loss about the spatial discretisation, which causes the organized interaction between the small scale vortexes not to be captured. This phenomenon is discussed by Cantwall [11].

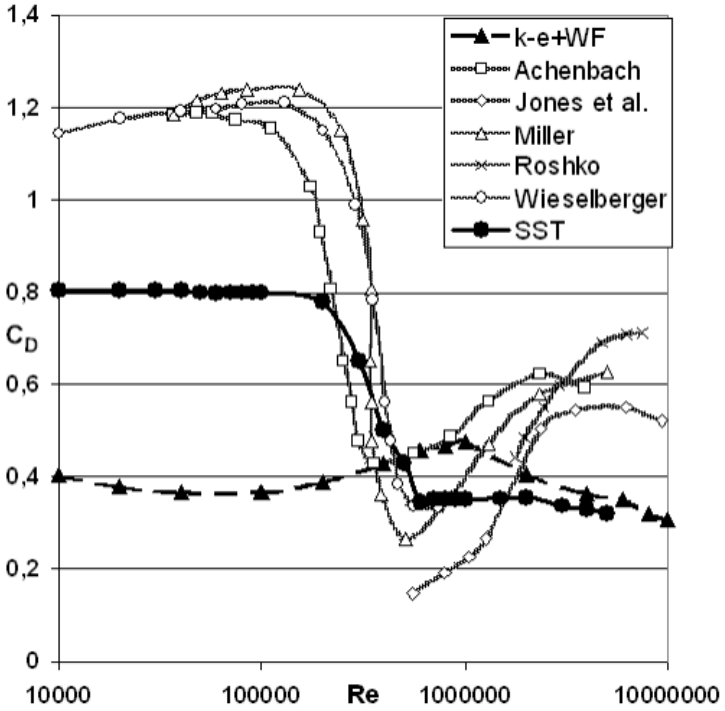

Figure 13: C_D vs. Re measurements and predictions. [7]

Figure 14 shows a snapshot of the vorticity occurring behind the cylinder computed by the present simulation. The image shows that the simulation is capable of capturing vortex shedding qualitatively quite well. It is also obvious from the figure that the width of the wake is smaller than the diameter of the cylinder, as stated by Roshko [26]. The velocity vectors close to the stagnation point illustrated in Figure 15 clearly shows that the boundary layer is turbulent, due to the shape of the velocity profile. This implies that the simulation is capable of modelling the turbulent nature of the boundary layer, which was uncovered by the experiments of Roshko [26].

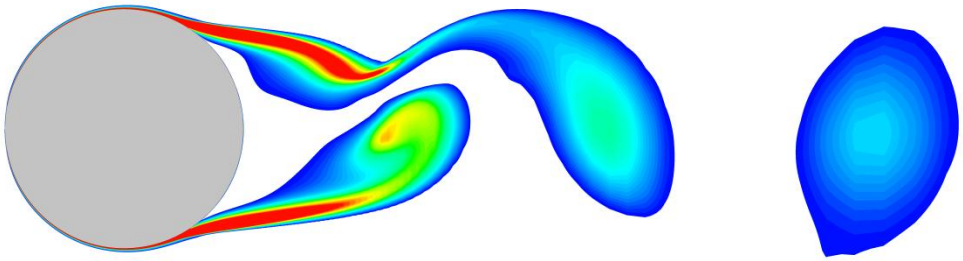

Figure 14: Snap shot of vorticity contours of flow around circular cylinder at the non-dimensional time step 159D/U_∞

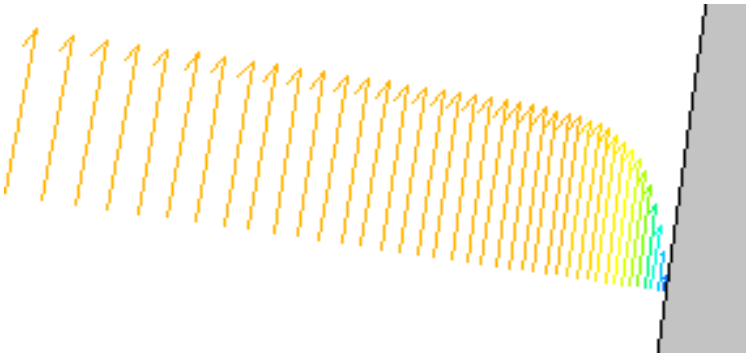

Figure 15: Image of velocity vector close to the stagnation point, at a peripheral angle of 5° on the cylinder wall.

The power spectra of the lift fluctuation in Figure 16 clearly show that the shedding regime is modelled with one distinct shedding frequency, this harmonizes with the power spectra obtained by Schewe [27], and illustrated in Figure 3.

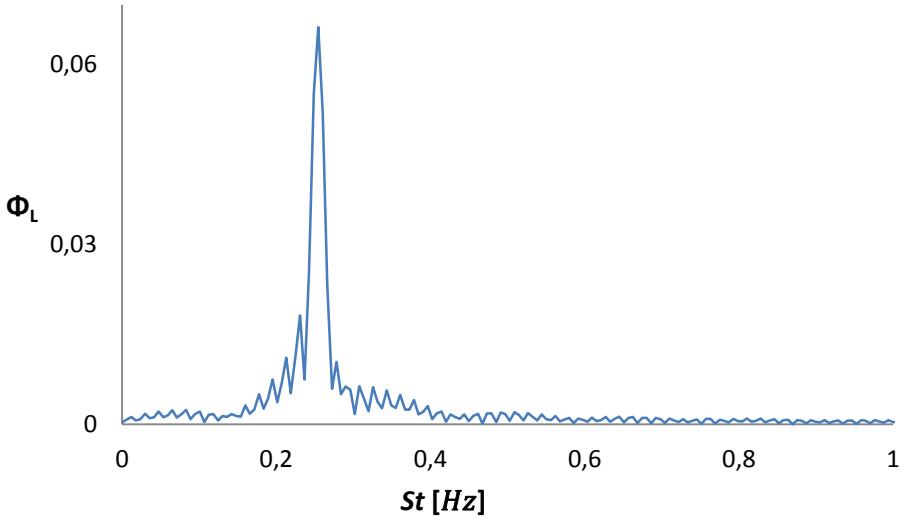

Figure 16: Power spectra of the lift fluctuations in transcritical regime

In Figure 17 the mean pressure distribution ($C_p = \{p_c - p_{c\infty}\}/\{0.5\rho U_\infty^2\}$) is plotted against the periphery angle around the cylinder wall. p_c is the static pressure measured along the cylinder surface, and $p_{c\infty}$ is the static flow pressure at infinity. Both numerical simulations underestimate the negative pressure on the back of the cylinder. This may be due to the large pressure gradients in this area, which is difficult to model accurately, and the real life occurrence of organized transient motions as mentioned previously [11]. Figure 18 shows the skin friction coefficient ($C_f = \tau/\{\rho U_\infty^2\}$) around the cylinder wall. The present simulation shows a quite large difference in the front half of the cylinder compared to Achenbach [1], but are quite similar at the back half. The boundary separation however is captured fairly well; whit a separation angel of $\theta_s = 117°$, compared to 115° in Achenbach's [1] experiments, and 114° in Ong et al. [25] simulations. The investigations of Shih et al. [30] shows that the skin friction coefficient is not modeled more accurate by the use of the Realizable turbulence model compared to the standard k-ϵ method, but the pressure distribution are shown to have an improved accuracy. The investigations performed by Achenbach [1] yields that the participation of skin friction in the total drag force at $Re = 3.6 \cdot 10^6$ is about 0.5%. One may therefore assume that the pressure distribution is determinant for the drag and lift forces. The reason for differences in the obtained drag coefficients from the present simulation, the one of Ong et al. [25] and the experiments of Achenbach [1] are displayed by the pressure differences on the back of the cylinder in Figure 17. A remark should also be made about the uncertainty of the two dimensional turbulence models ability to predict three dimensional effects, such as the pressure loss caused by local flow velocity in the span vise direction of the cylinder, and turbulent dissipation in the span vice direction.

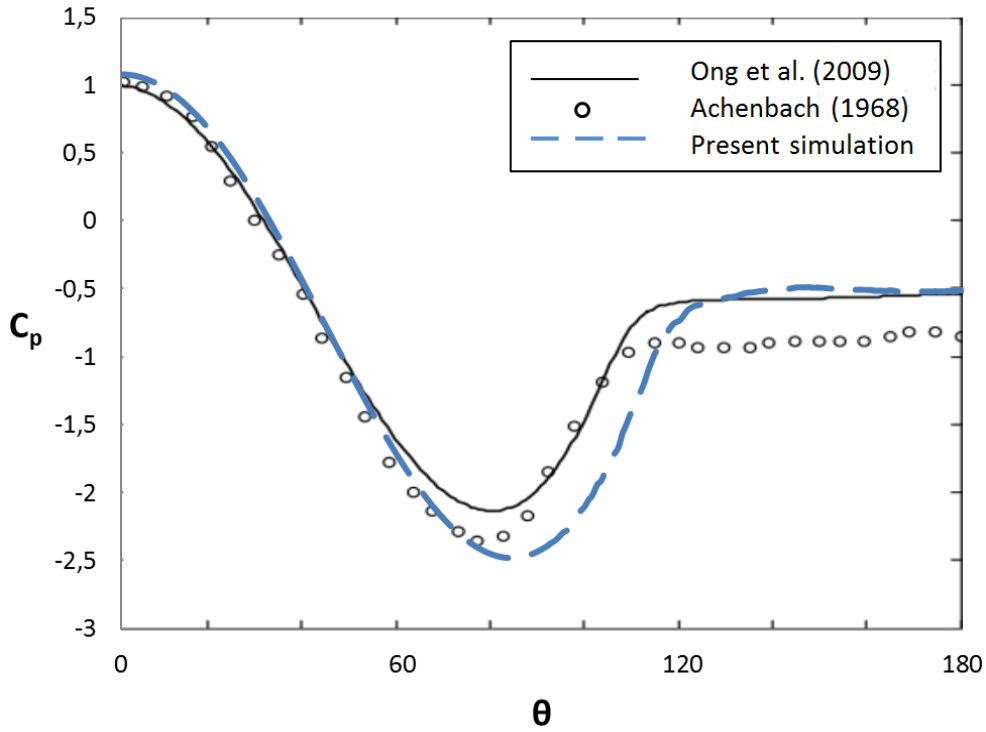

Figure 17: Mean pressure distribution along the cylinder wall with respect to the peripheral angle θ measured from the stagnation point.

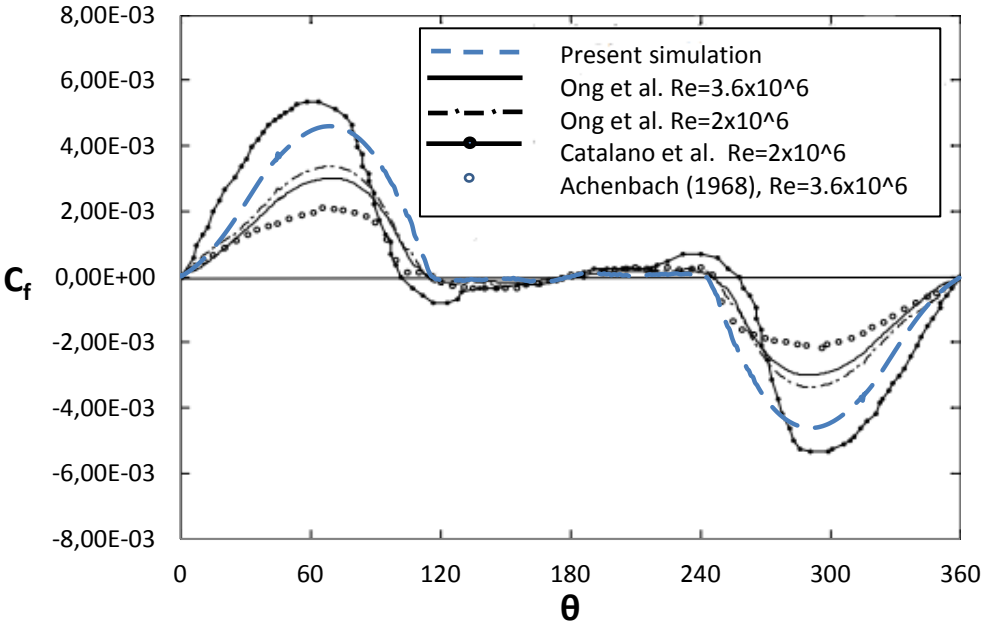

Figure 18: Skin friction distribution on cylinder surface

Concluding remarks & recommended further work

The results presented it this paper has shown the ability of URANS simulations to capture qualitatively the phenomenon of vortex shedding behind a circular cylinder in transcritical flow. This suggests that a coupling between a FEM analysis and a CFD analysis trough strip theory should be able to capture the effects of VIV on a submerged floating tunnel in the nearest future. However there are some challenges that need to be met.

The numerical analysis performed in this paper is a daring experiment due to lack of literature on the subject. There is need for a systematic investigation to be able to separate the grid resolution form the effects of wall-modeling. More numerical analysis is needed to examine different turbulence models, near wall treatments, and grid setup. Especially the non-conformal mesh used by Benim [7], illustrated in Figure 19, is very interesting for this problem, due to its ability to vary the y^+ value without varying the aspect ratio.

The present simulation was performed with $Re = 3.6 \cdot 10^6$, equivalent to a current velocity of $0.24[m/s]$, but as discussed earlier the tidal flow around a SFT may lead to $Re > 1.5 \cdot 10^7$, which is equivalent to a current velocity of $1.0[m/s]$. To raise the Reynolds number in the present simulation by a factor of four will lead to an increase in computation time to more than one month on a powerful personal computer. It will also be essential to be able to model a free cylinder subjected to current. Due to lack of computational resources, this was not investigated in the present study. Availability of large computational resources is therefore essential to be able to perform all the analysis needed to reduce the uncertainty of the numerically obtained results.

Turbulence models are developed using empirical results. It is therefore important to obtain experimental values in the transcritical range to validate the turbulence models accuracy for such simulations. Detailed experimental values are necessary to be able to confirm the flow modeling, especially more values for lift fluctuations and pressure distributions should be acquired from transcritical flows. To perform experiments at such high Re is very complicated and expensive. The most used experimental setup in the literature is a high pressurized wind tunnel.

The coupling used between the strip wise 2D CFD simulation and the 3D structural analysis by Schultz & Meling [28], is only based by the drag and lift forces. If the structural analysis is performed using a hydro elastic element, the coupling can consist of hydrodynamic quantities such as added mass and added damping, in addition to drag and lift forces. This could possibly increase the accuracy in the fluid structure interaction, and possibly reduce the number of CFD strips. The development of this technique also demands some physical experiment for validation purposes.

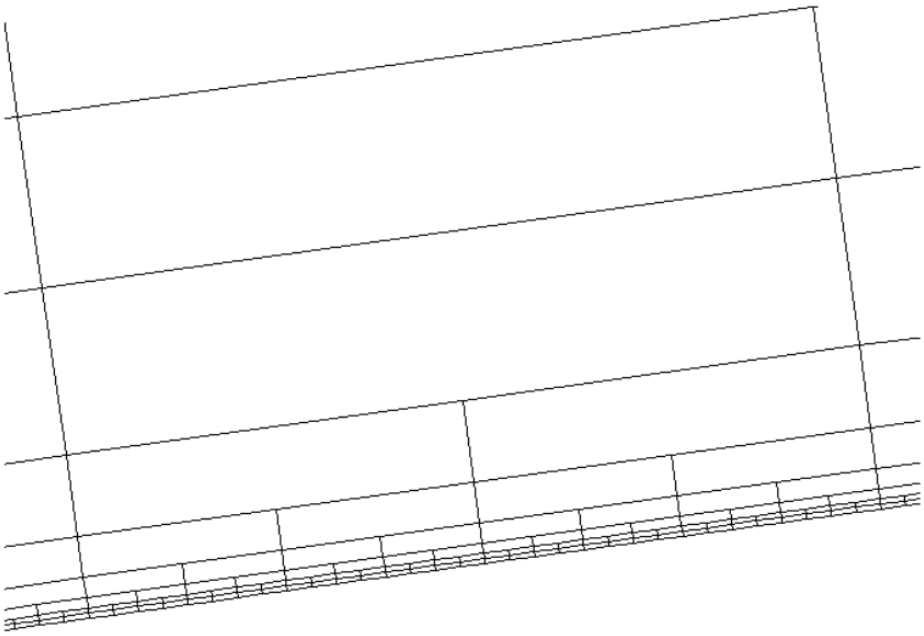

Figure 19: Detailed view of the non-conformal grid with hanging nodes used by Benim et al.[7]

References

[1] **Achenbach, E**. Distribution of local pressure and skin friction around a circular cylinder in cross-flow up to Re=5x10^6. *Journal of Fluid Mechanics* (1968), 625-639.

[2] **Achenbach, E and Heinecke, E**. *On vortex shedding from smooth and rough cylinders in the range of Reynolds number 6*10e3 to 5*10e6*. The Journal of Fluid Mechanics, 1980.

[3] **Andersson, H I, Gjerde, K M, and Jacobsen, Ø.** Turbulence and turbulence modelling. In *The first Scandinavian conference on viscous an turbulent flow in hydraulic machinery* (Trondheim 1987), SINTEF, Division of Fluid Dynamics, 1-34.

[4] **ANSYS, INC.** *ANSYS FLUENT Theory Guide*. Canonsburg, 2011.

[5] **ANSYS, INC.** *ANSYS FLUENT User Guide*. Canonsburg, 2011.

[6] **Barton, I E.** Comparison of SIMPLE- and PISO-type algorithms for transient flows. *International Journal for Numerical Methods in Fluids* (1998), 459-483.

[7] **Benim, A C, Cagan, M, Nahavandi, A, and Pasqualotto, E.** RANS Predictions Of Turbulent Flow Past a Circular Cylinder over the Critical Regime. In *International Conference on Fluid Mechanics and Aerodynamics* (Athen 2007), 232-237.

[8] **Bohl, W and Elmendorf, W.** *Technische Strömungslehre, 13. Ed.* Vogel, Würzburg, 2005.

[9] **Brandtsegg, A S.** *Dynamic analysis and modeling of floating bridges*. Trondheim, 2011.

[10] **Breuer, M.** A challenging test case for large eddy simulation: high Reynolds number circular cylinder flow. *International Journal of Heat and Fluid Flow.* (2000).

[11] **Cantwell, B J.** Organized Motion in Turbulent Flow. *Annual Reviews Fluid Mechanics* (1981), 457-515.

[12] **Catalano, P, Wang, M, Iaccarino, G, and Moin, Parviz.** Numerical simulation of the flow around a circular cylinder at high Reynolds numbers. *International journal of Heat and Fluid Flow* (2003), 463-469.

[13] **Coussirat, M.** *Theoretical/numerical study of flows with strong streamlines curvature.* Ph.D. Thesis, Universitat Pilitècnica de Catalunya, Barcelona, Spain, 2003.

[14] **Faltinsen, O.** *A comparison of frank close-fit method with some other methods used to find two-dimensional hydro-dynamic forces and moments for bodies which are oscillating harmonically in an ideal fluid.* Det Norske Veritas, Oslo, 1969.

[15] **Faltinsen, O M.** *Sea Loads on ships and offshore structures*. Cambridge University Press, Trondheim, 1990.

[16] **Greco, Marilena.** *TMR 4215: Sea Loads, Lecture Notes*. Trondheim, 2011.

[17] **Han, X, Sagaut, P, and Luco, D.** On sensitivity of RANS simulations to uncertain turbulent onflow conditions. *Elsevier, Computer & Fluids 61* (2012), 2-5.

[18] **James, W D, Paris, S W, and Malcolm, G V.** Study of viscous cross flow effects on circular cylinder at large Reynolds numbers. *American Institute of Aeronautics and Astronautics Journal* (1980), 1066-1072.

[19] **Jongen, T.** Simulation an Modeling of Turbulent Incompressivle Flows. *PhD thesis* (1992), Lausanne, Switzerland.

[20] **Launder, B E and Spalding, D B.** *Lectures in Mathematical Model of Turbulence.* Academic Press, London, 1972.

[21] **Mittal, S.** On the performance of high aspect ratio elements for incompressible flows. *Computational Methods in Applied Mechanics and Engineering 188* (2000), 269-287.

[22] **Morison, J. R.** *The force exerted by surface waves on piles*. Pet. Trans., 1950.

[23] **Newman, J.N.** *Marine Hydrodynamics*. M.I.T. Press., Massachusetts, 1977.

[24] **NORWEGIAN PUBLIC ROADS ADMINISTRATION.** A feasability study - How to cross the wide and deep Sognefjord. In *Attained 25.05.2012, from www.vegvesen.no*. http://www.vegvesen.no/_attachment/274047/binary/485789, 2011.

[25] **Ong, M C, Utnes, T, Holmedal, L E, Myrhaug, D, and Pettersen, B.** Numerical simulation of flow around a smoot circula rcylinder at very high Reynolds numbers. *Marine Structures 22* (2009), 142-153.

[26] **Roshko, A.** Experiments on the flow past a circular cylinder at very high Reynolds number. *Journal of Fluid Mechanics* (1961), 345-356.

[27] **Schewe, G.** *On the force fluctuations acting on a circular cylinder in cross flow from subcritical ut to transcritical Reynolds numbers*. The Journal of Fluid Mechanics, Göttinger, Germany, 1983.

[28] **Schulz, K W and Meling, T S.** Multi-strip Numerical Analysis of Flexible Riser Response. In *23rd International Conference on Offshore Mechanics and Arctic Engineering* (Vancouver, Canada 2004), 379-384.

[29] **Sharpkaya, T and Shoaff, R L.** *A discrete vortex analysis of flow about stationary and transversely oscillating cylinders.* Naval Postgraduate School, Montery, California, 1979.

[30] **Shih, T, Liou, W W, Shabbir, A, Yang, Z, and Zhu, J.** *A new k-e eddy turbulence model for high Reynolds number turbulet flows*. Elsevier Science Ltd., Cleveland, 1994.

[31] **Singh, S P and Mittal, S.** Flow past a cylinder: shear layer instability and drag crisis. *International Journal for Numerical Methods in Fluids* (2004), 75-98.

[32] **Smagorinsky, J.** General Circulation Experiments with the Primitive Equations. I. The Basic Experiment. *Monthly Weather Review Vol. 91* (1963), 99-164.

[33] **Sumer, B and Fredsøe, J.** *Hydrodynamics around cylindrical structures (Recised edition)*. World Scientific Publishind Co. Pte. Ltd., London, 2006.

[34] **Tutar, M and Holdø, A E.** Computational modelling of flow around a circular cylinder in sub-critical flow regime with various turbulence models. *International journal for Numerical Methods in Fluids* (2001), 763-784.

[35] **Versteeg, H K and Malalasekera, W.** *An introduction to Computational FluidDynamics, The Finite Volume Method*. Pearson Education Limited, Edinburgh, 1995.

[36] **Vugts, J. H.** *The hydrodynamic forces and ship motions in waves*. Ph.D. Thesis, TU Delft, 1970.

[37] **White, F. M.** *Viscous Fluid Flow*. McGraw-Hill, Inc. , 1991.

[38] **Wilcox, D C.** *Turbulence Modeling for CFD*. DCW Industries, Inc., California, 1998.

[39] **Wolfshtein, M.** The Velocity and temperature Dsitribution of One-Dimensional Flow with Turbulence Augmentation and Pressure Gradient. *International Journal of Heat Mass Transfer. 12.* (1969), 301-318.

[40] **Zdravkovich, M M.** *Flow around circular cylinders, vol. 1 fundemantals.* Oxford University Press, New York, 1997.

APPENDIX

Navier-Stokes equation

The basic equations for the derivation of Navier-Stokes equation is Newton' second law, the conservation of momentum. This equation is a statement regarding the changes of properties of the fluid particle related to time. To simplify the equations some notations will be explained, which can be found in the book of Versteeg & Malalasekera [35].

If one probes an arbitrary property denoted ϕ, which is a function of (x, y, t). The time derivative of this property, $D\phi/Dt$, can be written as

$$\frac{D\phi}{Dt} = \frac{\partial \phi}{\partial t} + \frac{\partial \phi}{\partial x}\frac{\partial x}{\partial t} + \frac{\partial \phi}{\partial y}\frac{\partial y}{\partial t}$$

The velocities of a fluid are denoted $\partial x/\partial t = u$, $\partial y/\partial t = u$, $\partial z/\partial t = w$, the equation can therefore be written as follows:

$$\frac{D\phi}{Dt} = \frac{\partial \phi}{\partial t} + u \cdot \frac{\partial \phi}{\partial x} + v \cdot \frac{\partial \phi}{\partial y} = \frac{\partial \phi}{\partial t} + \boldsymbol{u} \cdot \nabla \phi \qquad (17)$$

Where **u** is a vector consisting of the three velocity components; $\boldsymbol{u} = \{u, v\}^T$, and ϕ is any property which are a function of (x, y, t).

The general flow equations necessary to solve the problem at hand are the two dimensional Navier-Stokes equation for a Newtonian fluid. These equations may be derived in several ways. If one assumes that the fluid is incompressible, and temperature independent, the equations may be derived as such that one can exploit the reader's presumed solid mechanical background.

This derivation of the two dimensional Navier-Stokes equation for incompressible, Newtonian fluids, as performed by White [37], are constructed from:

- The conservation of mass equation
- Newton's second law
- The deformation law of a Newtonian fluid.
    - The fluid is continuous, and the strain is a linear function of the rate of change
    - The fluid is isotropic
    - The deformation law must reduce to hydrostatic pressure for zero rate of change

The conservation of mass can be obtained by considering a control volume with a height Δx_2 and a with Δx_1 and a unity depth, the mass inside the element

is equal to ($\rho\ \Delta x_1\ \Delta x_2$), for a incompressible fluid the rate of change of mass inside the element is zero, and can be written as:

$$\rho\Delta x_2 \cdot (\frac{\partial u_1}{\partial x_1}\Delta x_1) + \rho\Delta x_1 \cdot \frac{\partial u_2}{\partial x_2}\Delta x_2 = 0$$
$$\frac{\partial u_1}{\partial x_1} + \frac{\partial u_2}{\partial x_2} = 0 \qquad (18)$$

where u_1 and u_2 are velocities in horizontal and vertical direction respectively. With vector notation it can be further simplified:

$$\frac{\partial u_1}{\partial x_1} + \frac{\partial u_2}{\partial x_2} = \nabla \cdot \boldsymbol{u} = \mathbf{0} \qquad (19)$$

Where **u** is the velocity vector

Newton's second can be written as:

$$[\boldsymbol{F} = m\boldsymbol{a}] \cdot \frac{1}{V}$$
$$\rho\frac{D\boldsymbol{u}}{Dt} = \boldsymbol{f} = \boldsymbol{f}_{\boldsymbol{body}} + \boldsymbol{f}_{\boldsymbol{surface}} \qquad (20)$$

F and **a** are the force vector and acceleration vector respectively, V is the considered volume, **f** is the volume forces, which are split in to body forces, $\mathbf{f}_{\mathbf{body}}$ and the surface forces $\mathbf{f}_{\mathbf{surface}}$. The surface forces can be found by summing up all the forces acting on the element surface, see Figure 20

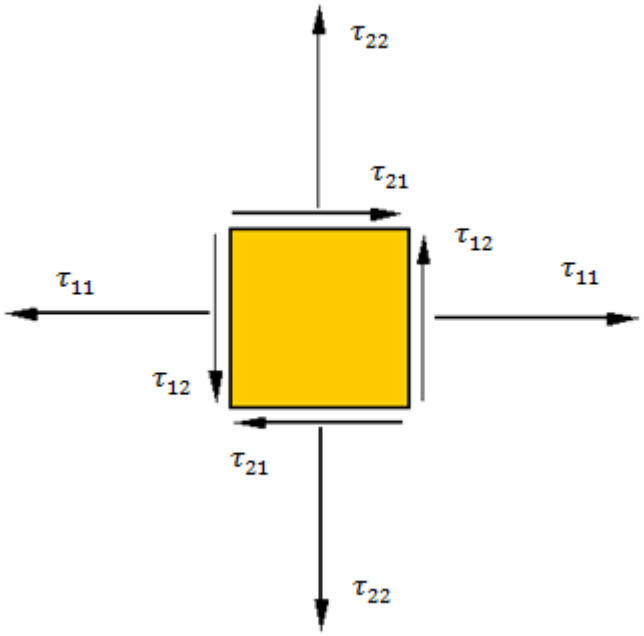

Figure 20: Stress components on all faces of a 2D fluid element

Because the fluid is isotropic $\tau_{ij} = \tau_{ji}$, the forces can be written as follows:

$$F_{surf,x_1} = \left(\frac{\partial \tau_{11}}{\partial x_1} dx_1\right) dx_2 + \left(\frac{\partial \tau_{12}}{\partial x_2} dx_2\right) dx_1$$

$$f_{surf,x_1} = \frac{\partial \tau_{11}}{\partial x_1} + \frac{\partial \tau_{12}}{\partial x_2} \qquad (21)$$

$$f_{surf,x\_i} = \frac{\partial \tau_{ij}}{\partial x_j}$$

where i,j=1,2.

To complete this derivation it is necessary to express the stresses in terms of the velocity. As stated by the deformation law of a Newtonian fluid, the stresses are linearly related to the rates of change in the fluid. As an analogy with the hookean elasticity theory, Stoke developed in 1845 the Stoke relations which states that the rate of change can be written as:

$$\epsilon_{ij} = \frac{1}{2}\left(\frac{\partial u_i}{\partial x_j} + \frac{\partial u_j}{\partial x_i}\right) \qquad (22)$$

The stresses are linearly dependent of eq.(22), and must reduce to the dynamic pressure, given by the Bernoulli equation, when the rate of change is zero. For an incompressible fluid it can therefore be written as:

$$\tau_{ij} = -p\delta_{ij} + \mu\left(\frac{\partial u_i}{\partial x_j} + \frac{\partial u_j}{\partial x_i}\right) \qquad (23)$$

where p is the dynamic pressure, and δ_{ij} is the kronecker delta function, and μ is the dynamic viscosity factor.

Using equation, (20), (21), and (23) Navier-Stokes equation can be formulated:

$$\rho \frac{Du_i}{Dt} = \frac{\partial}{\partial x_j}\left(-p\delta_{ij} + \mu\left(\frac{\partial u_i}{\partial x_j} + \frac{\partial u_j}{\partial x_i}\right)\right)$$

Using equation (19) yields:

$$\rho \frac{Du_i}{Dt} = -\frac{\partial p}{\partial x_i} + \mu \frac{\partial^2 u_i}{\partial^2 x_j} + f_{body} \qquad (24)\ a)$$

$$\rho \frac{D\boldsymbol{u}}{Dt} = -\nabla p + \mu \nabla^2 \boldsymbol{u} + \boldsymbol{f_{body}} \qquad (24)\ b)$$

$\mathbf{f_{body}}$ is in this case gravity forces, which is substantially smaller than the viscous forces, and can therefore be neglected, the equation then yields:

$$\rho \frac{D\boldsymbol{u}}{Dt} = -\nabla p + \mu \nabla^2 \boldsymbol{u} \qquad (25)$$

Reynolds equation

Using the relation in eq. (17), equation (24) a) can be written as:

$$\frac{\partial u_i}{\partial t} + u_j \frac{\partial u_i}{\partial x_j} = -\frac{1}{\rho}\frac{\partial p}{\partial x_i} + \nu \frac{\partial^2 u_i}{\partial^2 x_j} \qquad (26)$$

where ν is the kinematic viscosity which are defined as $\nu \equiv \mu/\rho$

This equation contains all necessary information for determining a time-dependent three-dimensional flow, including turbulence. However, the computation costs using these equations on a turbulent flow are immense. To reduce these costs, the Reynolds averaged equation is used. To obtain the Reynolds averaged equation, the properties in eq.(26) are rewritten as one average part, and one turbulent part.

$$\begin{aligned} u_i &= \overline{u}_i + u_i' \\ p &= \overline{p} + p' \end{aligned} \qquad (27)$$

$\overline{u}_i$ is the time average of u_i and u_i' is the turbulent part. The resulting equation obtained by introducing eq.(26) in to eq.(27), are then time-averaged, and the Reynolds averaged Navier-Stoke equation is obtained:

$$\overline{\frac{\partial(\overline{u}_i + u_i')}{\partial t}} + \overline{(\overline{u}_j + u_j')\frac{\partial(\overline{u}_i + u_i')}{\partial x_j}} = -\frac{1}{\rho}\overline{\frac{\partial(\overline{p} + p')}{\partial x_i}} + \nu \overline{\frac{\partial^2(\overline{u}_i + u_i')}{\partial^2 x_j}} \qquad (28)$$

$$\frac{\partial \overline{u}_i}{\partial t} + \overline{u}_j \frac{\partial \overline{u}_i}{\partial x_j} = -\frac{1}{\rho}\frac{\partial \overline{p}}{\partial x_i} + \nu \frac{\partial^2 \overline{u}_i}{\partial^2 x_j} - \frac{\partial \overline{u_i' u_j'}}{\partial x_j}_i$$

Note that the Reynolds averaged conservation of mass is given as:

$$\frac{\partial \overline{u}_i}{\partial x_i} = 0 \qquad (29)$$

Potential theory

As suggested by Newman [23]. By the use of potential flow theory only one equation needs to be found to solve for vectorial velocities, accelerations, and pressure. Basic assumptions for the potential flow theory are an inviscid fluid, which results in irrotational motion, and incompressible fluid. Neglecting elastic behavior of the fluid makes us able to deriving the governing equation:

$$\nabla V = 0, \text{ where } V = \nabla\phi \qquad (30)$$

The governing equation for the potential flow theory is then the Laplace equation:

$$\nabla^2\phi = 0 \qquad (31)$$

Boundary conditions:

- Impermeability of the sea bed:

$$\frac{\delta\phi}{\delta n} = 0 \text{ on } S_{SB} \qquad (32)$$

- Impermeability of structure:

$$\frac{\delta\phi}{\delta n} = V_B \cdot n, \text{ on } S_B \qquad (33$$

- Free surface kinematic condition:

$$\frac{\delta\phi}{\delta z} = \frac{\delta\zeta}{\delta t}, \text{ on } z = \zeta(x, y, t) \qquad (34)$$

- Free surface dynamic condition:

$$g \cdot \zeta + \frac{\delta\phi}{\delta t} = 0, \text{ on } z = \zeta(x, y, t) \qquad (35)$$

From these equations a potential can be derives, which describes velocity, accelerations and pressure in the volume Ω. Potential flow theory is not a god approximation for high sea states, since this involves nonlinear effects, but for a floating bridge, such sea states are not of importance. Comparisons done by Faltinsen [14] and Vugts [36] show that hydrodynamic quantities' can be found, with sufficient accuracy by potential theory. The only exception is the damping associated with the roll motion, where viscous effects play an important role

Morison's equation

Morison's formula is an empirical formulation describing the time averaged forces caused by current [22].

$$dF_i = \frac{1}{2}\rho C_i D\ dz\ |u_i|u_i \tag{36}$$

This equation gives the forces F_i acting on a strip with the length dz in the axial direction of the cylinder. C_1 is the drag coefficient C_D and C_2 is the lift coefficient C_L.

Y+ value

The y+ value is a non-dimensional distance between the first node and the nearest wall.

$$y^+ = \frac{u_* \Delta y}{\nu} \tag{37}$$

Where Δy is the first node height, ν is the kinematic viscosity and u_* is the friction velocity defined as:

$$u_* = \sqrt{\frac{\tau_w}{\rho}} \tag{38}$$

Where τ_w is the wall shear stress.